Molecular Dynamics Simulation of Amorphous Poly(ethylene terephthalate)

M. S. Hedenqvist,† R. Bharadwaj, and R. H. Boyd*

University of Utah, Departments of Materials Science and Engineering and of Chemical and Fuels Engineering, Salt Lake City, Utah 84112

Received September 24, 1997; Revised Manuscript Received January 2, 1998

ABSTRACT: A conformational energy model has been set up for poly(ethylene terephthalate) (PET) for use in molecular dynamics simulations. The molecular dimensions, as expressed by the characteristic ratio, and the dipolar correlation factor of PET are key parameters in the simulations because they depend very differently on the conformational characteristics of the individual bond types in the chain. These parameters as well as the equation of state of the melt were emphasized in testing the model, and satisfactory representation was accomplished. It was found, however, difficult to achieve the experimental glass volume in MD cooling experiments below T_g. Packing features of bulk PET are discussed in terms of radial distribution functions. Dipolar correlation was found to be largely intramolecular in nature.

Introduction

Poly(ethylene terephthalate) (PET) is a polymer that possesses a number of desirable properties. It can be prepared and used in both the amorphous and semicrystalline states and in varying conditions of orientation. It has found wide applications in films, fibers, and molded objects. As a result it has been very widely studied scientifically. Nevertheless, there is still much to be learned about the connection of its molecular structure to material properties. Atomistic simulations of polymer structure have reached the level where they are now useful in gaining insights into the molecular origins of behavior of bulk polymers.[1,2] The purpose of the present work is to initiate a molecular dynamics (MD) simulation of amorphous PET that can serve as the basis for investigations of the relation between materials properties and molecular structure in PET and related polyesters.

In recent MD simulations of other polymers[3−6] we have emphasized the role of pressure (P), volume (V), and temperature (T) properties as a sensitive monitor of the success of the assumed potential functions or force field, especially those associated with the nonbonded interactions, in mimicking the physical system. In the present simulation, we continue to place emphasis on adequate representation of the PVT properties as a prerequisite for meaningful simulation.

The solution dimensions of PET have been studied experimentally[7] and a rotational isomeric state (RIS) model has been developed by Flory,[8−10] which accounts for the measured characteristic ratio. This model serves as a useful starting point for the simulation system used here. PET is a polar polymer and as such has been studied dielectrically.[11,12] From the relaxed dielectric constant the dipolar correlation factor or dipole moment ratio for the bulk polymer is known.[12] This also serves as an important comparison for the simulation results. Because of their importance in building and assessing the model on which the simulation is based, a discussion of the characteristic ratio and dipole moment ratio in terms of RIS models and their relation to the measured values is taken up first and follows below. This discussion will also be central to interpretation of the results found in simulation.

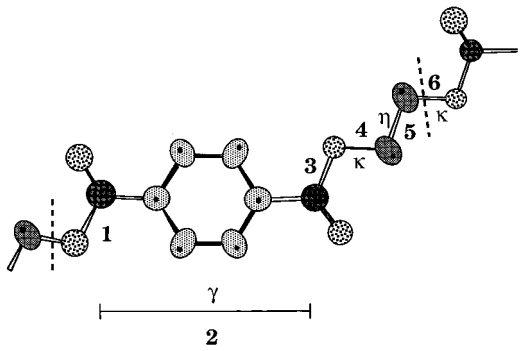

Figure 1. Repeat unit of PET, delineated by dashed lines. The bonds are numbered and also lettered according to type using the convention of Flory.[8] Bond type γ is an across ring virtual bond based on the torsional angle of the ester carbonyl groups, type κ is the C−O bond connecting the ester group to the ethylenic linkage, and η is the ethylenic C−C bond.

Rotational Isomeric State Representation of PET

First, a recount of the RIS model presented by Flory[8] is given. Figure 1 shows a PET repeat unit with the bonds numbered and designated by type with Greek letters according to the convention used by Flory. Bonds 1 and 3, in the ester group, are assumed to remain in the *trans* conformation and carry no energy weight parameter. Bond 2 is a virtual bond that spans the two ester sp^2 carbon atoms across the rigid benzene ring. The ester groups are assumed to be planar with the ring but can adopt *trans* or *cis* conformations with respect to each other. There is no *a priori* reason to assign greater weight to either conformation but a statistical weight parameter, γ, is assigned to the *cis* form. This is related to an energy of *cis* relative to *trans* of E_γ as $\gamma = \exp(-E_\gamma/RT)$. The C−O bonds (4,6) in the $-OCH_2-CH_2O-$ sequence are assigned a weight parameter σ_κ when in the *gauche* state vs unity in the *trans* state. Similarly, the C−C bond (5) in this sequence is given a

* Author to whom correspondence should be addressed.
† Present address: Packforsk, P.O. Box 9, S-164 93 Kista, Sweden.

S0024-9297(97)01412-5 CCC: $15.00
Published on Web 02/20/1998

weight σ_η when in the *gauche* state vs unity in the *trans*. Five-center or four-bond interactions, ω, are assigned at bond pairs 4,5 and 5,6. Thus there are four parameters characterizing the chain, the *cis*/*trans* energy difference, E_γ, two *gauche*/*trans* energy differences (E_{σ_κ} for C−O and E_{σ_η} for C−C bonds), and one bond pair interaction, E_ω. Of these, the *cis*/*trans* energy difference is expected to be zero.

The characteristic ratio, C_∞, is given by

$$C_\infty = \langle R^2 \rangle / \sum_i N_i l_i^2 \qquad (1)$$

in the limit of long chains where $\langle R^2 \rangle$ is the unperturbed mean-square end-to-end distance, N_i is the number of bonds of each of the six types in Figure 1 in the chain, and l_i is their length. Calculations of C_∞ using the above energy parameter formulation show that by assigning a slightly negative E_{σ_η} value that favors *gauche* at the C−C bond, a positive value to E_{σ_κ} at the C−O bonds, and a reasonable positive value to the four-bond interference, E_ω, along with zero *cis*/*trans* energy difference, E_γ, one can reproduce the experimental values of C_∞.[8] The particular statistical weights selected by Flory were $\gamma = 1.0$, $\sigma_\kappa = 0.5$, $\sigma_\eta = 1.5$, and $\omega = 0.10$.

From RIS calculations made here it is found that of the four statistical weight parameters, the characteristic ratio is most sensitive to the *gauche*/*trans* energy difference at the C−C bond. This is illustrated in Figure 2. There, C_∞ is plotted against E_{σ_η}/RT with the other parameters kept fixed at the Flory values. It may be seen that the characteristic ratio is quite sensitive to *gauche*/*trans* energy at the −C−C− bond. Apparently, this sensitivity is related to the C−C bond acting as an optimal geometric "pivot point" in causing large excursions of the ring to ring distances. It is seen also that slightly negative values of the E_{σ_η}/RT parameter, indicating a lower energy for the *gauche* conformation, are required to place C_∞ in the experimental range, i.e., at values of ~4.[7,10] The experimental values are unfortunately somewhat approximate, as they are based on viscosity measurements in good solvents, and corrections must be made to arrive at unperturbed dimensions. Flory and Williams[10] estimated values of 4.2 and 4.7 from two literature sources and an additional value in ref 7 is 3.7. Also shown in Figure 2 is the effect of variation of the *cis*/*trans* energy parameter, E_γ/RT, and the C−O bond *gauche*/*trans* parameter, E_{σ_κ}/RT. It may be seen that C_∞ is much less sensitive to the *cis*/*trans* and C−O *gauche*/*trans* energy parameters. The sensitivity of C_∞ to variations in ω parameters is similar to that for the *cis*/*trans* E_γ parameter.

A potentially useful companion to the characteristic ratio is the dipole moment ratio, D_∞. This is defined as

$$D_\infty = \langle \mu^2 \rangle / N_D m_0^2 \qquad (2)$$

in the limit of long chains where $\langle \mu^2 \rangle$ is the mean-square molecular moment, N_D is the number of dipoles (number of ester groups in this case), and m_0 is the moment of the ester group. The dipole moment ratio was not taken up previously,[8] no doubt because of a lack of appropriate experimental data on solutions. However, there is dielectric data available for bulk amorphous PET. The Kirkwood−Onsager equation (formulated in electrostatic units) expresses the dielectric constant of the bulk material in terms of local moments as[13]

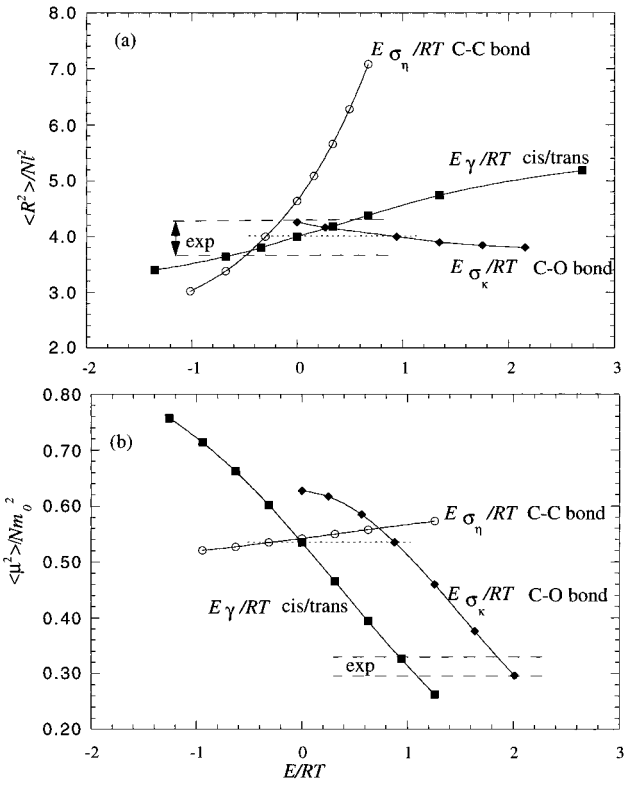

Figure 2. Results of RIS model calculations on PET. The characteristic ratio (panel a) and the dipole moment ratio (panel b) are plotted against reduced conformational energy parameters, E/RT. The plots represent the effect of variations of the three-bond interaction energies for the three bond types, γ, κ, and η (Figure 1). Each parameter is varied separately about a set of base parameters. The latter are given by $E_\gamma/RT = 0$, $E_\kappa/RT = 0.94$, and $E_\eta/RT = -0.30$, along with the four-bond parameter $E_\omega/RT = 1.35$. The intersections of the dotted lines with each of the curves indicate these base values as well as the values of characteristic and dipole moment ratios resulting from them. The vertical positions of the dashed curves indicate the range of experimental values. For the dipole moment ratio, the latter are inferred from bulk measurements.

$$\epsilon_R - \epsilon_U = \frac{3\epsilon_R}{(2\epsilon_R + \epsilon_U)}\left(\frac{\epsilon_U + 2}{3}\right)^2\left(\frac{4\pi \bar{N}_D}{3kT}\right) g m_0^2 \qquad (3)$$

where ϵ_R and ϵ_U are relaxed and unrelaxed dielectric constants, $\bar{N}_D$ is the number of dipoles per unit volume, m_0 is the dipole moment of the local group (i.e., ester group), and g is the correlation factor defined as

$$g = \sum_i \langle \vec{m} \cdot \vec{m}_i \rangle / m_0^2 \qquad (4a)$$

where $\vec{m}_i$ is a dipole in a large region, $\vec{m}$ is a central selected dipole, and the sum is over all dipoles in the region including the selected one. Alternatively, g can be written as

$$g = 1 + \sum_{i'} \langle \cos \theta_{i'} \rangle \qquad (4b)$$

where $\theta_{i'}$ is the angle between a dipole and the selected one and the sum over i' excludes the latter. When the molecular moment, $\vec{\mu}$, in eq 2 is expressed as a sum of local moments, $\vec{m}_i$, D_∞ reduces to a similar expression, except that the sum is over a chain. Thus, g differs from D_∞ in including the effects of *inter*molecular interaction

in addition to the *intra*molecular interactions implied in D_∞. The geometrical structure of the units in the chain and the conformational preferences of nearby bonds are the principal driving forces in determining D_∞. These same factors contribute to g, but in addition, there could be intermolecular packing effects that would result in intermolecular correlations. In general, it is often supposed that these would be weaker than the intramolecular effects driven by the chemical structure of the chain.

Experimentally, values of the Kirkwood correlation factor g can be deduced from dielectric measurements on amorphous PET in the temperature range 80−100 °C.[12] Below this temperature range, the process is at a very low frequency, and above it, PET crystallizes. Within this window, g values are found to lie in the range 0.28−0.32. The latter values are exceptionally small and are indicative of considerable negative correlation or antiparallel dipolar alignment in the important conformations of PET. These experimental values can be compared with values of the dipole moment ratio calculated according to the same RIS model and parameters as for the characteristic ratio. It appears to be a good approximation to regard the ester moment as pointing along the direction of the carbonyl group,[14,15] and the ester dipole is incorporated into the model as a vector pointing along the ester carbonyl bond.

The results of RIS model calculations made here of the dipole moment ratio are displayed in Figure 2. Several observations are to be made. In direct contrast to the characteristic ratio, it is found that the dipole moment ratio is quite insensitive to the *gauche*/*trans* ratio at the ethylene unit C−C bond and is very sensitive to the *cis*/*trans* ratio of the across ring ester groups and to the C−O bond *gauche*/*trans* parameter, E_{σ_k}/RT.

Since the ester groups are directly attached through the across-ring virtual bond, in all conformations about the across ring virtual bond the components of a pair of ester moments along the virtual bond cancel. Thus there is a conformation independent reduction of the correlation factor, to ∼0.75, from this feature. However, this reduction is modest in the context of the actual experimental value. In the *cis* configuration, the components of the dipoles perpendicular to the virtual bond are additive, and in the *trans*, they sum to zero. Therefore, the molecular moment is quite sensitive to the *cis*/*trans* ratio. The two C−O bonds play a sensitive role in determining the across diol correlation, the dipoles being antiparallel when the diol sequence is *trans* planar. The C−O bond role is enhanced by there being two such bonds compared to the one C−C bond. Further, and of most importance to the MD simulations of the bulk polymer carried out here, it is seen that calculated dipole moment ratios in the experimental range imply, from the *intra*molecular viewpoint, either values of the across ring *cis*/*trans* ratio lying on the side of favoring the *trans* configuration or values of the C−O bond σ_k parameter rather highly favoring the *trans* conformation. There is no *a priori* intramolecular structural reason to suppose the former circumstance. Thus it would seem that the *trans* conformation at the C−O bond is to be regarded as highly favored if, as is likely, intramolecular correlations dominate.

MD Simulation Details

PET Representation. The PET system consisted of a single chain with 60 monomer units (Figure 1). In order to decrease the computational burden, the methylene CH_2 units and the aromatic ring C−H units were represented by "anisotropic united atom" (AUA) groups.[16] In this formulation, the nonbonded potential force center is offset from the carbon atom along the C−H bond or the CH_2 bisector by a distance d. This distance is a parameter in addition to the well depth, ϵ, and size, σ, appearing in the spherically symmetric Lennard-Jones "6-12" potential. The offset has the effect of making the nonbonded potential appear anisotropic in comparison to one centered on the carbon atoms. No nonbonded interactions are included between 1,4 centers (3 bond interactions) as these are considered to be parameterized in the torsional potential. Atom centers are used for all other interactions including bond stretch, bond bend, torsional, and electrostatic. End units consisting of a CH_2(AUA) atom and a $-O-CH_2$(AUA) group were added to the left and right hand side, respectively, at the dashed lines of the repeating chain in Figure 1.

Molecular Dynamics Details. The simulations were generated using constant particle number, N, pressure, and temperature (NPT) dynamics. The Gear-predictor-corrector time integration method, used in concert with the Nosé extended system method for pressure and temperature control, in previous simulations[3−6] was found to be unstable on occasion and was replaced by the more robust velocity−Verlet algorithm.[17] We have also incorporated the Berendsen scaling methods (eqs 5 and 6) for temperature and pressure control.[18] At each time step, velocities are scaled by a factor (λ_T) given by

$$\lambda_T = \left[1 + \frac{\Delta t}{\tau_T}\left(\frac{T_o}{T_k} - 1\right)\right]^{1/2} \tag{5}$$

where Δt is the time step and τ_T is a time constant describing the rate at which the system reaches the desired temperature (T_o). T_k is the system temperature derived from the kinetic energy. At the same time the volume of the box is scaled by a pressure factor:

$$\lambda_P = 1 - \frac{\Delta t}{\tau_P}(P_o - P) \tag{6}$$

where τ_P, P, and P_o are the time constant, current pressure, measured from the virial, and desired system pressure, respectively. The pressure constant τ_P was set to 10^{-6} s atm and τ_T was taken to be 5 fs. Lower τ_P and τ_T values resulted in divergence of the time integration, and higher values yielded too long equilibration times. The time step was 1 fs.

The packed system was initially created by placing an all-*trans* chain in a large periodic cubic box (box side = 700 Å). The box was subsequently shrunk to equilibrium size at high temperature, 650 K. The box was shrunk in a number of steps using NPT dynamics, starting at a moderate imposed pressure and continuing at increasingly lower pressures. At each step, after a smaller volume was established in a fairly short time the system was allowed to equilibrate further at constant volume under NVT dynamics (using large τ_P values). Finally, the system was equilibrated at 1 atm under NPT conditions. Lower temperature systems were obtained by cooling this initial system. Volume equilibration, as judged by the volume being constant in time, was obtained by observing trajectories for at least 1 ns at each temperature.

Phantom chain calculations were also carried out. These were accomplished on a continuous unwrapped chain of the same 60 monomer units with no periodic boundary conditions. Nonbonded and electrostatic interactions farther away than one monomer unit along the chain contour were switched off.

The computations were carried out on IBM RS6000/560 and -/370 and Sun Sparc Ultra 170E workstations as well as on a Silicon Graphics Power Challenge XL computer.

Potential Functions. In so far as possible, the valence force field parameters were taken from those used in previous MD and molecular mechanics studies. This includes parameters used for the methylene unit in polyethylene[6] (PE) and other polymers, the aromatic ring in polystyrene[3] (aPS), and the ester group in aliphatic polyesters.[15,19,20] PET differs from previous work in that the ester group is attached to the aromatic ring. The ester group thus required some parameter selection beyond that in an all aliphatic environment. The work of Hummel and Flory[21] was primarily used in accomplishing this. Bond stretching and bending constants are based on spectroscopically determined values. As has been common practice, the stretching constants are reduced by a factor of 4 in order to increase the time step. Because the aliphatic sequence $-CH_2-CH_2-$ occurs in the ethylene oxide moiety, it has some special characteristics. There is uncertainty with respect to the relative stabilities of the *gauche* and *trans* conformations in this situation. In molecules containing the $O-CH_2-CH_2-O$ sequence, such as dimethoxyethane and poly(ethylene oxide) (PEO), it has often been considered that there is a "*gauche*" effect and that the *gauche* conformation is more stable than *trans*. As discussed above, the Flory rotational isomeric model calculations for PET adopted a statistical weight favoring the *gauche* conformation slightly, by ~1 kJ mol^{-1}. There is recent evidence from *ab initio* quantum mechanical calculations that the effect in PEO is actually due to a bond conformation triplet interaction of the type $TG^{\pm}G^{\mp}$ and that the *gauche*/*trans* energy difference actually favors the *trans* slightly.[22] Other quantum mechanical calculations of the barriers and conformational energies have been made.[23] In view of the problematic nature of whether these conclusions apply to the sequence in PET and the apparent necessity seen in the results in Figure 2a for favoring *gauche*, we have chosen to explicitly include *gauche* favoritism in the torsional potential. The intrinsic three-fold barrier to rotation was selected to be the same as in PE and the Flory value for the *gauche* vs *trans* stability incorporated by means of an appropriate single-fold torsional potential term. The torsional potential at the ester O−C bond (CD−O−C−C sequence; see Table 1 for the atom symbol notation) gives a total barrier of 3.5 kJ mol^{-1}, compared to 2.25 kJ mol^{-1} used by Smith and Boyd.[15] The one-fold term favors the *trans* conformation. In addition, it was found that the five-center ω type interaction due to nonbonded interactions suppresses *gauche* conformations at this bond. An explicit out-of-plane deformation term was included to maintain planarity at the ester group. Table 1 lists the constants and their sources.

The nonbonded potential for the $-CH_2-$ group was the previously used AUA potential.[6] The explicit atom carbon and oxygen ester group nonbonded potentials were taken from Sorensen et al.[24] In previous work on aPS, a potential of the AUA form was invoked for the

Table 1. Potential Functions[a]

Bond Stretch Energy = $(1/2)k_R(R - R_0)^2$

	k_R	R_0
O−C[b]	774	1.41
O−CD[c]	782	1.33
CA−CD[d,e]	661	1.49
CA−CA[d]	1130	1.39
OD−CD[c]	1430	1.22
C−C[b]	646	1.53

Bond Bending Energy = $(1/2)k_\theta(\theta - \theta_0)^2$

	k_θ	θ_0 (deg)
CD−O−C[c]	422	109.47
O−CD−CA[e]	422	114.0
O−CD−O[c]	602	120.0
CA−CA−CD[e]	422	120.0
OD−CD−CA[e]	343	124.0
CA−CA−CA[d]	602	120.0
O−C−C[b]	498	109.47

Torsional Potentials

$(1/2)V_2[1 - \cos(2\phi)] + (1/2)V_1[1 + \cos(\phi)]$

	V_2	V_1
CA−CD−O−C[f]	58.6	16.7
OD−CD−CA−CA[g]	10.5	0
CA−CA−CA−CD[h]	54.4	0
CA−CA−CA−CA[d]	108.8	0

$(1/2)V_3[1 + \cos(3\phi)] + (1/2)V_1[1 + \cos(\phi)]$

	V_3	V_1
CD−O−C−C[i]	0.21	3.35

$(1/2)V_3[1 + \cos(3\phi)] + (1/2)V_1[1 - \cos(\phi)]$

	V_3	V_1
O−C−C−O[i]	13.4	1.38

Out of Plane Bending Potential = $(1/2)k_\delta\delta^2$

	k_δ
O−CD−CA···OD*[j]	361

Nonbonded Potential[k] $V(r) = 4\epsilon[(\sigma/r)^{12} - (\sigma/r)^6]$

	ϵ	σ	d
$-CH_2-$(AUA)	0.686	3.51	0.42
−O−	0.837	2.851	0.0
>CD−	0.397	3.34	0.0
>CA(H) (AUA)	0.536	3.65	0.3
−OD	0.837	2.851	0.0

Electrostatic Potential[l]

	q
$-CH_2-$	0.063
−O−	−0.126
>CD−	0.333
−OD	−0.270

[a] Energies in kJ mol^{-1}, distances in Å, angles in radians (shown above as degrees). The notation is as follows: C = sp^3 carbon; CD = sp^2 carbon; CA = aromatic carbon; O = divalent oxygen; OD = carbonyl oxygen. [b] Reference 24. [c] Reference 15. [d] Reference 3. [e] Reference 21. [f] From ref 15 assuming that the barrier for maintaining planarity in the ester group is the same as for an all aliphatic ester, C−CD−O−C. [g] There are two such terms set up for each ester group to phenyl ring connection, for a total barrier of 21 kJ mol^{-1}.[21] [h] Two torsion terms serve to maintain planarity at the CD to CA attachment with the total taken to be the same as the in-ring terms, CA−CA−CA−CA. [i] See text. [j] Out-of-plane deformation of doubly bonded oxygen OD from the plane of the O−CD−CA atoms in the ester group. The constant was increased by a factor of 2/3 above the value of ref 15 in order to keep the ester group more rigidly planar. [k] The "*d*" parameter is the offset of the Lennard-Jones force center from the carbon atom center. For a CA center bonded to CD, *d* is taken to be zero. [l] *q* values are partial charges in units of |*e*|, the electron charge, from ref 15. See text for the distance dependent dielectric constant parameters.

aromatic carbon CA−H group.[3] In its parametrization it was found that good *PVT* results were obtained with the offset parameter, *d*, near zero and a value of $d = 0$ was adopted. In the initial stages of the current work it was found that the specific volumes in simulation were too low. As a consequence, the aromatic carbon CA−H united atom nonbonded potential was modified to correct this deficiency. The well depth, ϵ, was kept the same, and various values of increasing offset, *d*, parameter were tried in combination with decreasing size parameters, σ. The values $d = 0.3$ and $\sigma = 3.65$ Å compared with $d = 0$ and $\sigma = 3.76$ Å used for aPS) were adopted on the basis of fits to experimental specific volumes at 600 and 650 K. All of the nonbonded parameters are listed in Table 1.

The electrostatic energy was based on fixed partial charges located at the carbon and oxygen atoms at the polar CD═O, CD−O, and O−C bonds of the ester group as

$$V(r_{ij}) = \frac{1}{4\pi\epsilon_o}\sum_{i<j}\frac{q_i q_j}{\epsilon(r_{ij})r_{ij}} \qquad (7)$$

The charges were taken from dipole moment computations on small molecule esters.[15] Polarization effects were incorporated via a distance dependent dielectric constant,[25−28]

$$\epsilon(r_{ij}) = 1 \qquad r_{ij} < r_e$$
$$= \epsilon_B e^{-(r_e/r_{ij})\ln(\epsilon_B)} \qquad r_{ij} > r_e \qquad (8)$$

The form of the latter is based on a Debye screening model. The resulting distance dependent dielectric constant is taken to be 1 below a critical radius, r_e, and approaches the bulk dielectric constant, ϵ_B at large *r*. The latter was taken to be 3.18, the experimental unrelaxed dielectric constant.[12] The critical radius is based upon the idea that, within the distance of an atom diameter, there is no screening. The critical radius was taken as the average nonbonded potential σ value for the actual PET system ($r_e = 3.5$). We have closely followed the details given by Smith et al.[28] in implementing the method. This includes forcing the electrostatic force to zero at a truncation radius and beyond. This is accomplished by using a five-degree switching polynomial to describe the electrostatic potential. The polynomial also gives a smooth splice at the critical radius, r_e.

Five-center interactions and higher were considered in the electrostatic and the Lennard-Jones nonbonded interactions. The truncation radius was set to 9.0 Å for both types of potentials. Continuum corrections for truncation of nonbonded energy and pressure were applied but were not necessary for the electrostatic contributions due to the truncation method described above.

PVT Behavior

***PVT* Results for PET Melts.** Specific volumes at 1 atm versus time at a number of the temperatures studied are shown in Figure 3. The curves were taken after the initial equilibration and the points represent 10 ps averages. The average volume at each temperature in the melt region is plotted against temperature in Figure 4. Also shown are the experimental results at 1 atm of Zoller and Bolli[29] for molten PET. The specific volume vs pressure at 597 K is shown in Figure 5 along with the experimental results of Zoller and

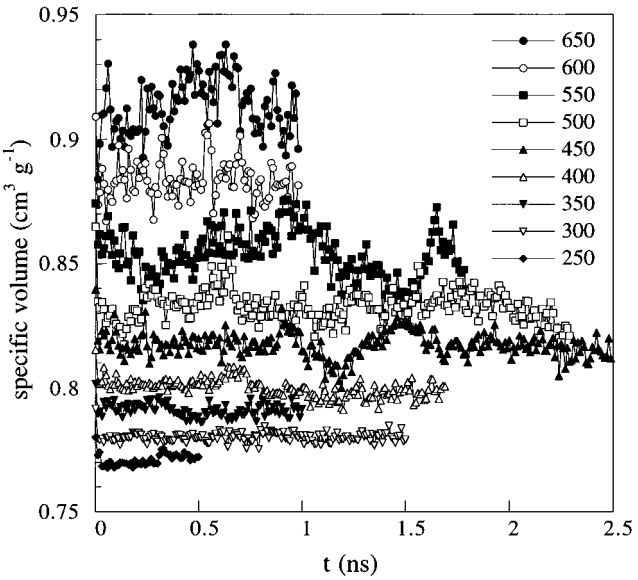

Figure 3. Specific volume vs time in MD runs for a number of the temperatures studied. The points are 10 ps averages.

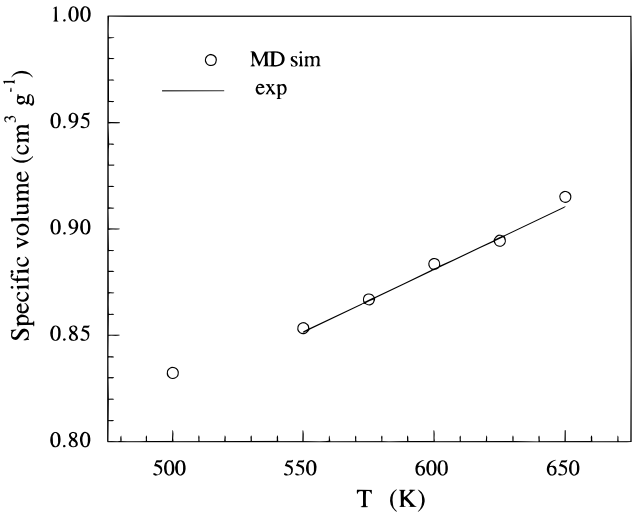

Figure 4. Specific volume vs temperature at 1 atm in the melt region. The points are MD results, and the line represents the experimental results of Zoller and Bolli.[29]

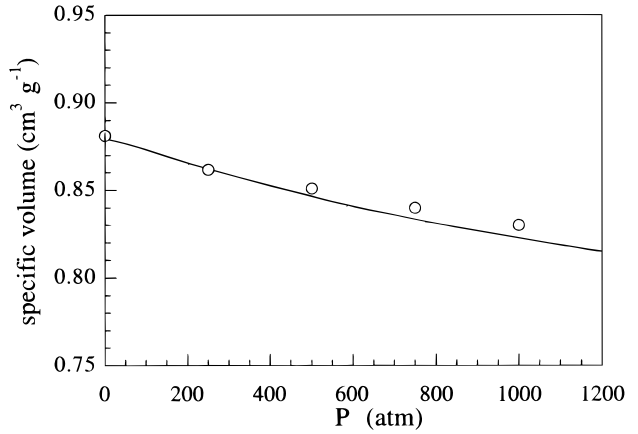

Figure 5. Specific volume vs pressure at 597 K. The points are MD results, and the curve represents the experimental results of Zoller and Bolli.[29]

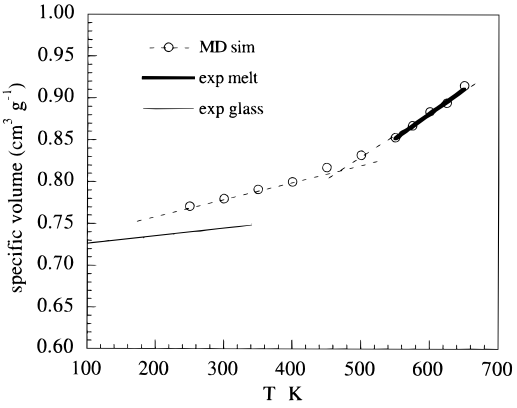

Figure 6. Specific volume vs temperature at 1 atm over the entire temperature range studied. The points are from MD simulation. The dashed lines are an aid in delineating the melt and glass regions in the simulation results. The heavy line is the experimental results of Zoller and Bolli[29] for the melt, and the thin line is the experimental results of Coburn and Boyd[12] for the glass.

Bolli.[29] The agreement of the simulation for the 1 atm isobar in the melt with the experimental results is good. This, of course, reflects the efficacy of the adjustment of the Lennard-Jones parameters for the united-atom aromatic carbon centers as well as the suitability of the other nonbonded parameters. The 597 K isotherm in Figure 5 agrees fairly well with experiment, although some tendency for the compressibility from simulation to be less than experimental at higher pressures is discernible.

***V*−*T* Behavior and PET Glass.** Specific volumes at 1 atm from MD simulation over a wide temperature range, from the melt down to below room temperature are shown in Figure 6. The experimental volume data of Zoller and Bolli[29] for the melt and the results of Coburn and Boyd[12] for the glass are also displayed. The onset of vitrification is evident in the MD results as a change in thermal expansion in the vicinity of 450 K. However, it is also evident that the volume from simulation lies above the experimental glass volume and that the thermal expansion in the glass from simulation is higher than experimental. The value of T_g inferred from simulation (region of 450 K) is considerably higher than the experimental value of 350 K. Presumably, all of these effects are attributable to the relatively short equilibration times (a few ns) in MD simulation. The situation with respect to being able to reach values of the glass volume close to experiment in MD simulation is unclear. In previous work on aPS[3] and atactic polypropylene (aPP),[5] this was accomplished. But in *cis*-polybutadiene (cisPBD),[4] polyisobutylene (PIB),[30] and amorphous PE[6] the experimental glass volumes were not available. For aPP, aPS, *cis*-PBD, and PIB the values of T_g from MD generated $V-T$ curves were found to be displaced upward in temperature relative to experiment.[31] However, the displacements were smaller than experienced here for PET.

Solubility Parameter. The solubility parameter, δ, is closely connected to the equation of state behavior since both depend rather directly on the nonbonded energy functions. This parameter was calculated from the simulation results as $\delta = (\Delta E/V)^{1/2}$, where ΔE is the cohesive energy and V is the volume. The cohesive energy was taken to be the intermolecular nonbonded and electrostatic energy. Solubility parameter values thus determined from simulation as a function of temperature are presented in Figure 7. There are tabulated values for δ based on correlations with refractive index and dipole moment available for PET. The value derived by Koenhen and Smolders,[32] also shown in Figure 7, is quite consistent with the MD simulation values, especially when it is considered that the MD values for the glass specific volumes are somewhat high, Figure 6.

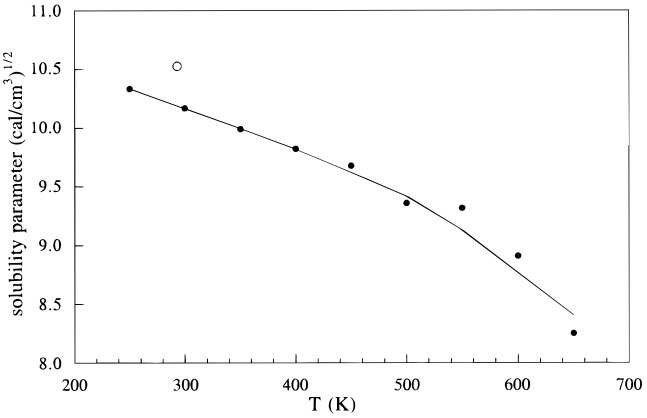

Figure 7. Solubility parameter of amorphous PET as a function of temperature from MD simulation (filled points). The curve smooths the results. The open circle is a value deduced from refractive index and dipole moment correlations by Koenhen and Smolders.[32]

Structural Characterization

Comparison with X-ray Scattering Experiments. X-ray diffraction experiments provide a potential source of information about structural features of the melt or glass. There is such a study for PET glass. The differential radial distribution function (DRDF) obtained by Fourier transformation from X-ray diffraction[33] is given by

$$4\pi r^2\bar{\rho}H(r) = \frac{2r}{\pi}\int_0^\infty si(s)\,\sin(rs)\,ds \qquad (9)$$

where $\bar{\rho}$ is the average atom density, i.e., the total number of atoms divided by the system volume, r is the radius, s is the scattering vector, and $i(s)$ is the interference function. The MD-sampled DRDF is computed using

$$H(r) = \sum_{i=1}^{3}\sum_{j=1}^{3}\frac{x_i x_j f_i f_j}{(\sum_{i=1}^{3} x_i f_i)^2}(g_{ij}(r) - 1) \qquad (10)$$

where $g_{ij}(r)$ is the radial distribution function of atom type j from atom type i (C, O, and H). x_i and f_i are the number fraction and scattering factor of the i-type atom. The scattering factors were considered radially dependent by using exponential expressions to describe experimental scattering factor data.[34] Since H atoms were absent in the MD simulations, these were constructed from geometries of existing atoms and subsequently implemented in the scattering calculations.

The scattering results of Gupta and Yeh[35] are compared with the MD-generated scattering function in Figure 8. Although the resolution of the experimental results is not very high, there is good general agreement concerning the features. The peaks at ∼1.5 and ∼2.5 Å are obviously associated with bond lengths and

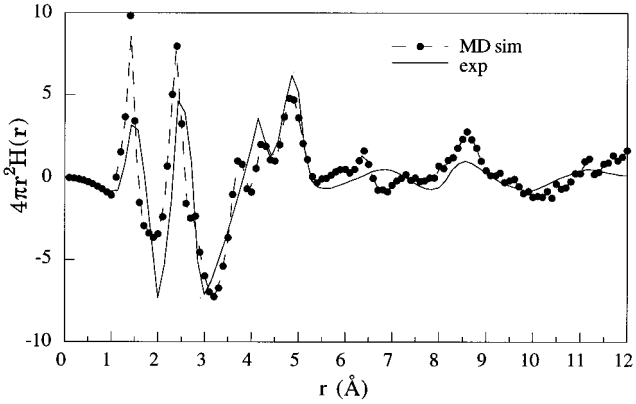

Figure 8. Differential radial distribution function, eq 9, plotted against distance. The points and dashed curve are from MD simulation, and the solid curve is the experimental results of Gupta and Yeh.[35]

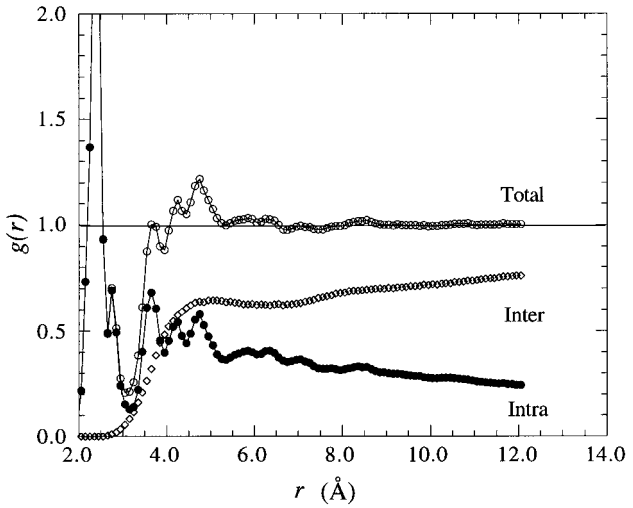

Figure 9. Radial distribution function for PET at 400 K. The complete function is also shown decomposed into intra- and intermolecular contributions.

valence angles, respectively. A shoulder at ∼2.8 Å arises from cis three-bond distances involving the aromatic ring carbons and also the ester group. The features at 3.5−5.0 Å arise from four-bond distances or five-bond distances across the aromatic ring. From 5 to 9 Å there are features due to six- and seven-bond distances. Finally, beyond 10 Å a broad peak due to monomer unit to monomer unit periodicity can be discerned.

Radial Distribution Functions. In addition to the comparison of the MD DRDF with the experimental X-ray result made above, it is of interest to examine the total radial distribution function and the various site−site RDFs, $g_{ij}(r)$, in terms of structural features, especially those related to *inter*molecular packing. A site−site $g_{ij}(r)$ may be decomposed into *inter*- and *intra*-molecular contributions by "unwrapping" the periodic box chain coordinates into a continuous chain. Two centers whose unwrapped coordinates represent the closest periodic image constitute intramolecular interactions; otherwise, they are inter. The resolution of the total RDF into intra and inter contributions at 400 K is shown in Figure 9. A diffuse peak at ∼5 Å is apparent for the intra and inter contributions at 400 K is shown in Figure 9. A diffuse peak at ∼5 Å is apparent for the inter function in Figure 9. This represents the interchain spacing, as is made more clear in Figure 10. In this figure the inter function is further decomposed into site−site RDFs based on the ethylenic moiety, containing the C atom type, and the terephthalic acid residue composed of the CA, CD, OD, and O atom types (Table 1). The interchain spacing is especially apparent in the −C−C− function where a second maximum can be seen and is reminiscent of the function for polyethylene.[6]

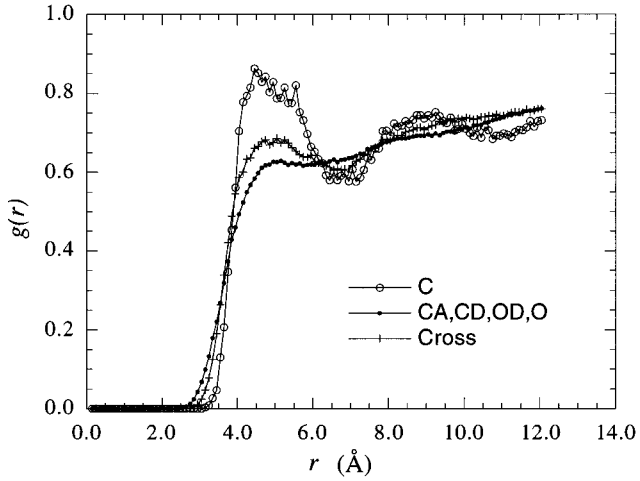

Figure 10. Site−site intermolecular radial distribution functions based on the ethylene linkage to ethylene linkage (C atom types, Table 1) and the terephthalic acid residue to terephthalic acid residue (CA, CD, OD, and O atom types). Also shown is the cross function between the two types of groups.

Characteristic Ratio and Dipolar Correlation Factor Behavior

As indicated in the section above on the RIS model representation of PET, the unperturbed dimensions as expressed by the characteristic ratio and dipole moment ratio or dipolar correlation factor form an important testing ground for the conformational energy model adopted and its attendant potential energy parameters. The bulk polymer is expected to form a "Θ solvent" that displays unperturbed dimensions behavior. Thus, a comparison of the dimensions in the bulk with the experimental characteristic ratio inferred from solution dimensions would be in order. The characteristic ratio in a simulation is to be determined directly from eq 1 by sampling of R^2. Because of the periodic boundary conditions, R distances are meaningful only for values of less than half the periodic box size, in this case ∼26/2 = ∼13 Å. In previous simulations[3−6,30] this has been sufficient to allow extrapolation of $\langle R_{ij}^2\rangle/N$ for various $N = |i - j|$ values, where i and j are indices of a reference atom in various repeat units along the chain, vs N in order to determine a fairly accurate value of C_∞. In the present case this is not possible because the repeat unit itself is so large that only a few units exceed the limit set by periodic boundary conditions. Therefore, a direct comparison of dimensions from simulation in the bulk with experiment is not possible. However, it is possible to carry out the simulation under phantom conditions without the periodic boundary conditions and arrive at a characteristic ratio that can be compared with experiment. Values of the characteristic ratio were determined from plots of sampled $\langle R_{ij}^2\rangle/N$ vs chain length for a 60 monomer unit chain without periodic boundary conditions and with all but shorter range nonbonded and electrostatic interactions switched off. Figure 11 shows the result of a 4 ns MD simulation. A characteristic ratio of ∼3.8 is indicated, a result consistent with literature values in the vicinity of 4.[7,10]

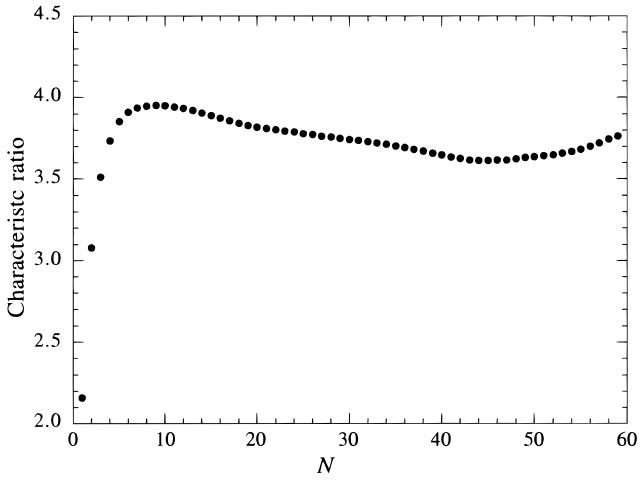

Figure 11. Characteristic ratio of a 60 monomer unit PET phantom chain as a function of chain length. The values shown are based on all monomer separations, $|i - j|$, equal to N. From MD simulation at 375 K.

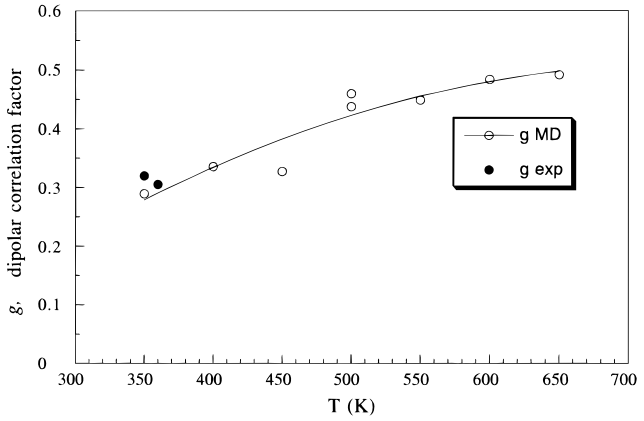

Figure 12. Dipolar correlation factor for bulk PET from MD simulation as a function of temperature. Experimental values[12] for the bulk are also shown.

In principle, the dipole moment ratio could be subject to the same problem from the periodic boundary conditions. However, due to the "perpendicular" nature of the moment vectors, it converges vs chain length much more rapidly than the end-to-end distance. Bulk values of this quantity, directly sampled according to eq 2, should be representative of a large system. In Figure 12 the dipole moment ratio is plotted vs temperature for the bulk system. The dipole moment ratio or dipolar correlation factor, g, agrees well with the experimental value at the appropriate temperature. The g factor from simulation is fairly temperature sensitive. This appears to be due to the effect of temperature on the *trans* conformation population at the "κ" type C−O bonds, 4 and 6 in Figure 1. As seen in Figure 2, the dipolar correlation factor is quite sensitive to the preferences at these bonds. Table 2 lists a comparison of bond populations at several temperatures in the bulk. The *trans* population of the 4,6 C−O bond decreases as temperature increases. This circumstance is no doubt the inevitable effect of temperature on the more highly populated species.

Finally, some remarks on the importance of intermolecular vs intramolecular correlation on the dipole moment ratio are in order. The discussion of the latter in the context of the RIS model above was inherently connected with intramolecular effects. However, the

Table 2. Effect of Temperature on Bond Populations in Bulk PET, Expressed as *trans* Fraction[a]

temp (K)	bonds 1,3 CD−O ester *trans* vs *cis*	bond 2 across ring *trans* vs cis	bonds 4, 6 (C−O) *trans* vs *gauche*	bond 5 (C−C) *trans* vs *gauche*
400	1.0, 1.0	0.51	0.79, 0.75	0.44
575	1.0, 1.0	0.48	0.72, 0.73	0.46
625	1.0, 1.0	0.51	0.70, 0.71	0.46

[a] The bond numbers refer to Figure 1.

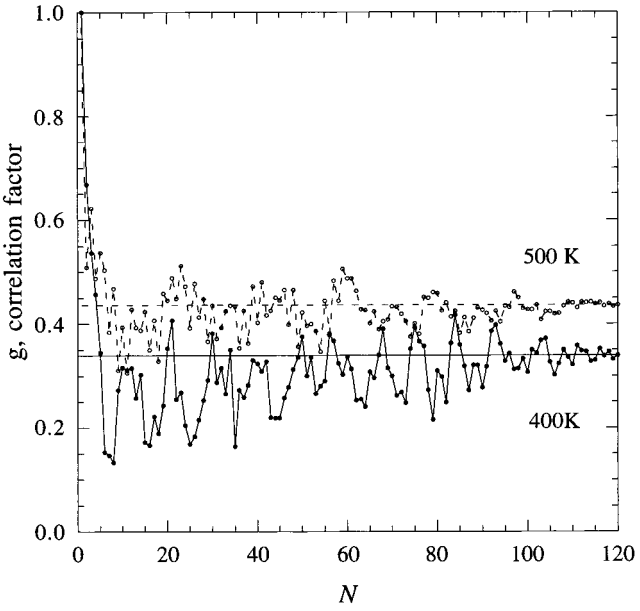

Figure 13. Convergence of the dipole−dipole correlation in bulk PET as a function of dipole separation along the chain. Each point, N, represents the contribution of all dipoles with separation, $|i - j|$, less than N.

role of intermolecular correlation needs to also be addressed. It appears that an effective way of doing this is to examine the convergence in MD sampling of the sum in eq 4 as the interval between monomers increases. This is done in Figure 13 in terms of the contribution of all dipole separations, $|i - j|$, less than N, where i and j are integers labeling the dipoles sequentially along the chain (120, in all, in the 60 monomer system). Smaller values of N are to be associated with intramolecular correlation, and larger ones are likely to be intermolecular in nature, even though there is no guarantee of clean separation. It may be seen that convergence is quite rapid, especially at 500 K. There is some overshoot at 400 K at small N values that could indicate some positive correlation associated with intermolecular interaction that partially compensates for the negative intramolecular contributions. Overall, however, it appears that the dipolar correlation factor for PET can largely be explained in terms of intramolecular correlations.

Acknowledgment. We are indebted to the Eastman Kodak Co. for financial support of this work and to J. M. O'Reilly and D. Perchak for their help and interest. The Sweden-American Foundation and the Swedish Institute are gratefully acknowledged for support that made this work possible for M.H. The Polymers Program, Division of Materials Research of the National Science Foundation, has provided support for computational facilities and our simulation efforts, and the Center for High Performance Computing (CHPC) at the

University of Utah is thanked for providing additional computer time.

References and Notes

(1) *Atomistic Modeling of Physical Properties of Polymers*; Monnerie, L., Suter, U., Eds.; Springer: Berlin, 1994.
(2) Boyd, R. H. *Trends Polym. Sci.* **1996**, *4*, 12.
(3) Han, Jie; Boyd, R. H. *Polymer* **1996**, *37*, 1797.
(4) Gee, R. H.; Boyd, R. H. *Polymer* **1995**, *36*, 1435.
(5) Han, J.; Boyd. R. H. *Macromolecules* **1994**, *27*, 5365.
(6) Pant, P. V. K.; Han, J.; Smith, G. D.; Boyd, R. H. *J. Chem. Phys.* **1993**, *99*, 597.
(7) Kurata, M.; Tsunashima, Y. Viscosity-Molecular Weight Relationships and Unperturbed Dimensions of Linear Chain Molecules. In *Polymer Handbook*, 3rd ed.; Brandrup, J., Immergut., E. H., Eds.; Wiley-Interscience: New York, 1989.
(8) Flory, P. J. *Statistical Mechanics of Chain Molecules*; Wiley: New York, 1969.
(9) Flory, P. J.; Williams, A. D. *J. Polym. Sci., Polym. Phys. Ed.* **1967**, *5*, 399.
(10) Williams, A. D.; Flory, P. J. *J. Polym. Sci., Polym. Phys. Ed.* **1967**, *5*, 417.
(11) For reviews see: (a) Boyd, R. H. *Polymer* **1985**, *26*, 323. (b) McCrum, N. G.; Read, B. E.; Williams, G. *Anelastic and Dielectric Effects in Polymeric Solids*; Wiley: New York, 1967.
(12) Coburn, J. C.; Boyd R. H. *Macromolecules* **1986**, *19*, 2238.
(13) Fröhlich, H. *Theory of Dielectrics*; 2nd ed.; Clarendon Press: Oxford, U.K., 1958; Chapter II.
(14) Saiz, E.; Hummel, J. P.; Flory, P. J.; Plavsic, M. *J. Phys. Chem.* **1981**, *85*, 3211.
(15) Smith, G. D.; Boyd, R. H. *Macromolecules* **1990**, *23*, 1527.
(16) Toxvaerd, S. *J. Chem. Phys.* **1990**, *93*, 4290.
(17) Allen, M. P.; Tildesley, D. J. *Computer Simulation of Liquids*; Clarendon Press: Oxford, U.K., 1987.
(18) Berendsen, H. J. C.; Postma, J. P. M.; van Gunsteren, W. F.; DiNola, A.; Haak, J. R. *J. Chem. Phys.* **1984**, *81*, 3684.
(19) Smith, G. D.; Boyd, R. H. *Macromolecules* **1991**, *24*, 2731.
(20) Liau, W. B.; Boyd, R. H. *Macromolecules* **1990**, *23*, 1531.
(21) Hummel, J. P.; Flory, P. J. *Macromolecules* **1980**, *13*, 479.
(22) (a) Smith, G. D.; Yoon, D. Y.; Jaffe, R. L. *Macromolecules* **1993**, *26*, 5213. (b) Jaffe, R. L.; Smith, G. D.; Yoon, D. Y. *J. Phys. Chem.* **1993**, *97*, 12745. (c) Smith, G. D.; Jaffe, R. L.; Yoon, D. Y. *J. Phys. Chem.* **1993**, *97*, 12752.
(23) Lautenschläger, P.; Brickmann, J.; van Ruiten, J.; Meier, J. *Macromolecules* **1991**, *24*, 1284.
(24) Sorensen, R. A.; Liau, W. B.; Kesner, L.; Boyd, R. H. *Macromolecules* **1988**, *21*, 200.
(25) Block, H.; Walker, S. M. *Chem. Phys. Lett.* **1973**, *19*, 363.
(26) Andrea, T. A.; Swope, W. C.; Andersen, H. C. *J. Chem. Phys.* **1983**, *79*, 4576.
(27) Rutledge, G. C.; Suter, U. W. *Macromolecules* **1991**, *24*, 1921.
(28) Smith, G. D.; Jaffe, R. L.; Yoon, D. Y. *Macromolecules* **1993**, *26*, 298.
(29) Zoller, P.; Bolli, P. *J. Macromol. Sci., Phys.* **1980**, *B18*, 555.
(30) Pant, P. V. K.; Boyd, R. H. *Macromolecules* **1993**, *26*, 679.
(31) Han, J.; Gee, R. H.; Boyd, R. H. *Macromolecules* **1994**, *27*, 7781.
(32) Koenhen, D. M.; Smolders, C. A. *J. Appl. Polym. Sci.* **1975**, *19*, 1163.
(33) Pings, C. J.; Waser, J. *J. Chem. Phys.* **1968**, *48*, 3016.
(34) Alexander, L. E. *X-ray Diffraction Methods in Polymer Science*; Wiley: New York, 1969.
(35) Gupta, M. R.; Yeh, G. S. Y. *J. Macromol. Sci., Phys.* **1978**, *B15*, 119.

MA9714124